Validation of Beamforming Techniques for Interference Mitigation in GNSS Handheld Receivers with Skydel Simulator

Lucía Pallarés-Rodríguez, Gonzalo Seco-Granados, and José A. López-Salcedo
Dept. of Telecommunication and Systems Engineering, IEEC-CERES, Universitat Autònoma de Barcelona (UAB)
Barcelona, Spain

***Abstract*—Global Navigation Satellite Systems (GNSS) are the primary technology for delivering reliable positioning and timing solutions, supporting a wide range of applications across different sectors. However, their performance can be significantly degraded by interference, which gives rise to the need for robust countermeasures that ensure both accuracy and resilience. This paper presents a testbed based on the Skydel GNSS Software Simulator for conducting multi-antenna GNSS experiments under real-world conditions, enabling interference mitigation studies without the need for additional hardware. The output is adjusted and sent to the FGI-GSRx GNSS software receiver, which evaluates the impact of the beamforming algorithms across all receiver stages, providing a comprehensive assessment of their effect on positioning performance. Two well-known techniques, Power Inversion (PI) and Capon (CAP), are analyzed within the context of small receivers, with results demonstrating their potential for interference mitigation even with limited antenna arrays, thus proving their suitability for handheld devices.**

***Index Terms*—Global navigation satellite system, Skydel, Array processing, Interference, Handheld, Capon, Power Inversion.**

I. Introduction

Global Navigation Satellite Systems (GNSS) play a crucial role in modern society, serving as a key technology across a wide range of sectors [1]. A major threat to this service arises when interference, whether intentional or not, appears, causing inaccuracies in the positioning solution or disrupting the receiver's performance [2], [3]. This issue has grown significantly in recent years, mainly due to the lower cost and increased accessibility of jamming devices, emphasizing the need to enhance the robustness of GNSS receivers and develop effective countermeasures against this threat [4]–[6].

Extensive research has been conducted to counteract interference effects [7]–[9], with spatial diversity emerging as a particularly promising approach [10]. The deployment of multiple antennas at the receiver enables the extraction of the spatial characteristics of incoming signals, allowing the system to filter out undesired contributions based on their spatial properties. Numerous studies have explored the feasibility of array processing techniques for interference mitigation, comparing the performance of well-known algorithms in this new context and proposing novel beamforming solutions to address the specific challenges of the GNSS domain [11]–[14].

However, most of the existing research assumes the use of large antenna arrays, leaving the issue of GNSS handheld receivers, such as smartphones and tablets, largely unexplored. The main limitation in these devices lies in space constraints, which substantially limit the integration of multi-antenna techniques. To accurately deploy the algorithms, an antenna separation of $\lambda/2$ between consecutive elements must be maintained. For GPS L1 signals, this translates to an inter-element distance of approximately 10 cm. This poses a significant challenge for small devices, where the overall size is often comparable to this value, restricting the number of antennas that can be deployed. Evidently, reducing the number of antennas also decreases the effectiveness of beamforming techniques, as the number of coefficients or weights applied in the spatial filter directly corresponds to the available antenna elements. Recent research has analyzed the effect of different beamforming algorithms on small antenna arrays in interference scenarios [15], [16]. However, these studies typically provide results in terms of attenuation capacity or focus primarily on blind beamforming approaches, which, while simpler to implement, generally yield worse results than algorithms that rely on *a priori* known information.

With this in mind, the aim of this paper is twofold. First, we present a testbed based on the Skydel GNSS Software Simulator for conducting multi-antenna experiments without the need for additional hardware. By configuring various features of Skydel, we emulate the behavior of a GNSS receiver equipped with an antenna array, enabling the analysis of diverse beamforming techniques under real-world conditions. The output of the simulator is then fed into the FGI-GSRx GNSS software receiver [17], which allows us to evaluate the impact of the applied algorithms across all receiver stages, offering a comprehensive view of the effect of beamforming.

Second, based on the proposed architecture, we evaluate the performance of two well-known techniques, Power Inversion (PI) [18] and Capon beamformer (CAP) [19]. Although these techniques have been studied for decades in the context of interference mitigation, the goal of this work is to assess their suitability for small GNSS receivers, providing positioning-level results obtained under real-world conditions, thus demonstrating the potential of beamforming even with small arrays.

This work has been partly supported by the Spanish Agency of Research (AEI) under grant PID2023-152820OB-I00 funded by MICIU/AEI/10.13039/501100011033 and by ERDF/EU, and grant PDC2023-145858-I00 funded by MICIU/AEI/10.13039/501100011033 and by the European Union NextGenerationEU/PRTR.

II. Beamforming Techniques for Interference Mitigation

A. Signal Model

Let us consider a L-element antenna array that receives the line-of-sight (LOS) contributions from V visible satellites along with M undesired components. The perceived signal by the L antennas at time instant n can be modeled as a $L \times 1$ vector, $\mathbf{x}[n]$, that follows the subsequent baseband discrete-time signal structure,

$$\mathbf{x}[n] = \sum_{v=1}^{V} \mathbf{a}(\varphi_v, \theta_v) s^{(v)}[n] + \sum_{m=1}^{M} \mathbf{a}(\varphi_m, \theta_m) i_m[n] + \mathbf{n}[n], \tag{1}$$

where $s^{(v)}[n]$ is the desired signal coming from satellite v, $i_m[n]$ is the m-th interference, and $\mathbf{n}[n]$ denotes the i.i.d. Gaussian noise. The spatial signature introduced by the array for a contribution with direction of arrival (DoA) (φ_j, θ_j) is denoted by the steering vector $\mathbf{a}(\varphi_j, \theta_j) \in \mathbb{C}^{L\times 1}$, where φ_j and θ_j indicate the azimuth and elevation of the j-th source, respectively.

B. Beamforming Techniques

The spatial samples encompassed in $\mathbf{x}[n]$ are linearly combined through a set of coefficients or weights, $\mathbf{w}$, which exploit the spatial characteristics of the different signals impinging the antenna array to filter out the undesired contributions. This process is mathematically described as,

$$y[n] = \mathbf{w}^H \mathbf{x}[n], \tag{2}$$

with $(\cdot)^H$ indicating the Hermitian transpose and $y[n]$ defining the output of the beamformer.

The computation of these weights is carried out according to a predefined criterion, which determines the beamforming technique in use and its effectiveness. Depending on the characteristics of the received undesired contributions, the mitigation capacity of a given technique can vary, particularly due to the level of correlation between these components and the desired GNSS signals. In the presence of general interference, such as intentional jammers or any uncorrelated contributions that might degrade the quality of service, GNSS receivers can easily benefit from conventional and straightforward beamforming approaches. In this work the focus is placed on two well-known techniques, the PI beamformer and the CAP beamformer, which have been extensively proposed to address the challenges of GNSS interference.

1) Power Inversion (PI) Beamformer: The idea behind the PI beamformer is to minimize the overall received power at the output of the beamformer, $P_y = \mathbb{E}\{|y[n]|^2\}$. To achieve this while ensuring that not all weights are zero, the weight associated with the reference antenna is set to one, $[\mathbf{w}]_1 = 1$, thereby guaranteeing that $\mathbf{w} \neq 0$. This results in the following solution for the optimum weights of the PI beamformer,

$$\mathbf{w}_{\text{PI}} = \frac{\mathbf{R}_{\mathbf{x}}^{-1}\boldsymbol{\delta}_1}{\boldsymbol{\delta}_1^H \mathbf{R}_{\mathbf{x}}^{-1}\boldsymbol{\delta}_1}, \tag{3}$$

where $\mathbf{R}_{\mathbf{x}}$ is the spatial covariance matrix estimated after processing N samples as $\mathbf{R}_{\mathbf{x}} = \frac{1}{N}\sum_{n=0}^{N-1} \mathbf{x}[n]\mathbf{x}^H[n]$.

2) Capon (CAP) Beamformer: The CAP beamformer, also referred to as Minimum Variance Distortionless Response (MVDR) beamformer, designs the weights in order to minimize the power at the output while keeping a distortionless constraint in the DoA of the desired signal. This guarantees that at the DoA of the satellite under evaluation, v, the array response will be equal to one, $\mathbf{w}^H\mathbf{a}(\varphi_v, \theta_v) = 1$, ensuring that the weights do not alter the signal impinging from the specified direction. Whereas this provides benefits in terms of phase preservation and C/N_0 levels for the GNSS signals, it implies computing a set of weights for all visible satellites, i.e., for each DoA. Taking this into consideration, the CAP weights associated with the v are obtained as,

$$\mathbf{w}_{\text{CAP}}^{(v)} = \frac{\mathbf{R}_{\mathbf{x}}^{-1}\mathbf{a}(\varphi_v, \theta_v)}{\mathbf{a}^H(\varphi_v, \theta_v)\mathbf{R}_{\mathbf{x}}^{-1}\mathbf{a}(\varphi_v, \theta_v)}. \tag{4}$$

III. Testbed Architecture and Configuration

Both previously introduced techniques are widely recognized and have been extensively studied in the field of array processing for a considerable time. Most of the reported analysis rely on the attenuation values introduced by the beamformers to characterize their performance. However, while the mitigation capacity demonstrates the potential of PI and CAP for interference suppression, a more comprehensive understanding is obtained by analyzing more relevant performance metrics, such as the accuracy of the positioning solution. In this work, we carry out this evaluation under particularly constrained conditions, considering a very limited number of antennas –at most four– thus assessing the capabilities of beamforming techniques in smaller GNSS devices.

To conduct the analysis, we use the Skydel GNSS Software Simulator to generate a representative scenario in which the GNSS signals are affected by a strong interference. Leveraging Skydel's features, we simulate a multi-antenna receiver using multiple instances of the application, subsequently processing the retrieved signals through a module where the proposed techniques are applied. This module yields the output samples described in (2), where the signal is supposedly interference-free, hence the last step is to obtain a positioning solution. For this purpose, we use the FGI-GSRx GNSS receiver, which enables the processing of the output signal, providing acquisition, tracking and navigation performance indicators. A diagram illustrating this architecture is presented in Fig. 1.

A. Spatial Diversity with Skydel Simulator

The Skydel simulator generates the transmitted signals in the form of I/Q data, which can either be fed into a software-defined radio (SDR) to generate RF signals or stored for direct processing in their I/Q form. As shown in Fig. 1, we directly process the I/Q files generated by Skydel, avoiding the need for additional hardware.

In order to replicate the behavior of a multi-antenna receiver, we make use of multiple Skydel instances. Each of them shares exactly the same simulation parameters, with

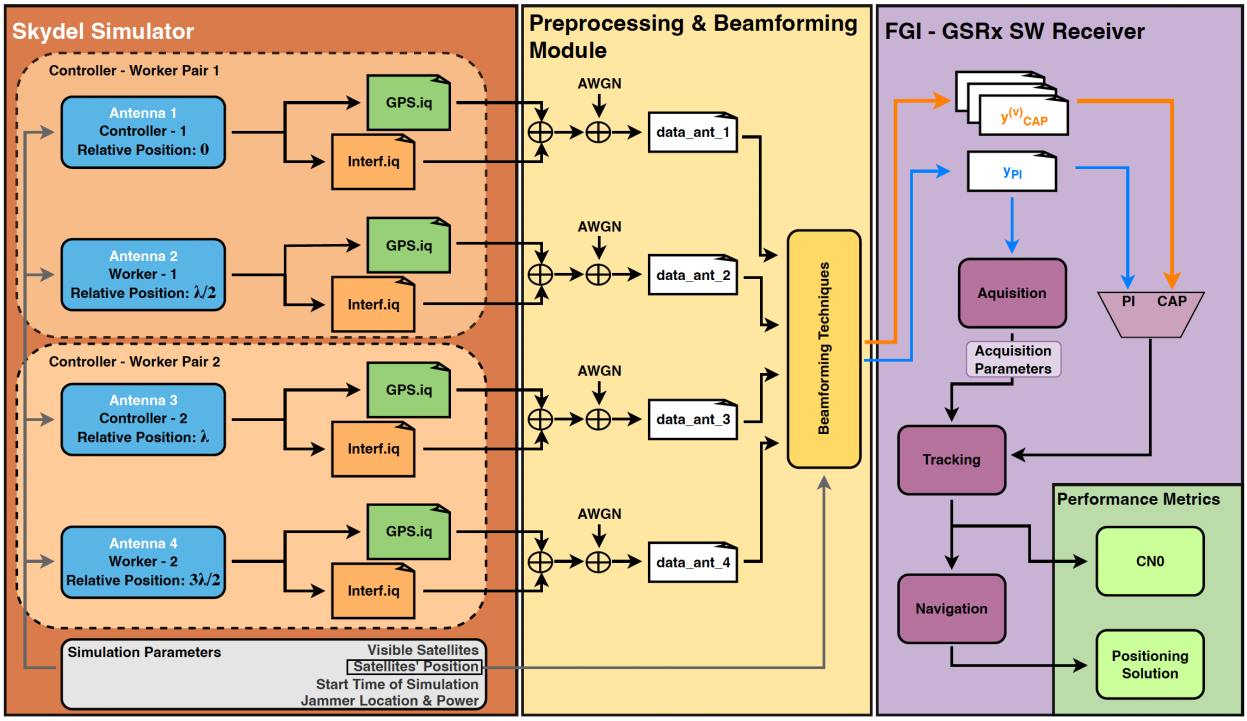

Fig. 1. Diagram illustrating the process followed for the experiments.

the exception of the receiver's position, which is shifted by a distance of $\lambda/2$ between consecutive antennas to model the required inter-element separation of a real multi-antenna receiver. Considering the first instance as the reference antenna, the receiver's position at each subsequent instance must be displaced by a distance of $l\frac{\lambda}{2}, l = 2, \ldots, L-1$. In our system, we are restricted to running only two simultaneous instances, synchronized using the controller-worker paradigm offered by Skydel. Therefore, the first controller-worker pair is executed to model the first two antennas, followed by a second controller-worker pair that recreates the behavior of the third and fourth elements. Note that all mentioned processes must share the exact same simulation parameters, except for the receiver's position, to ensure a proper characterization of a device equipped with an antenna array.

From the GNSS perspective, we exclusively use the GPS constellation. Specifically, we focus on the L1 signals from the visible satellites shown in the sky view in Fig. 2. The positions of the satellites with respect to the receiver, in terms of azimuth (φ) and elevation (θ), are provided by Skydel, thus we use this information to construct the distortionless constraint for the CAP weights in the beamforming module.

The interfering source is introduced into the simulation using Skydel's "Advanced jammer" setting. The key distinction of this feature compared to the "Basic interference" is that it allows specifying the position of the transmitter, thereby incorporating spatial information about the interference into the simulation. This is a crucial aspect for our analysis, since the mitigation capabilities leverage the spatial signature of the

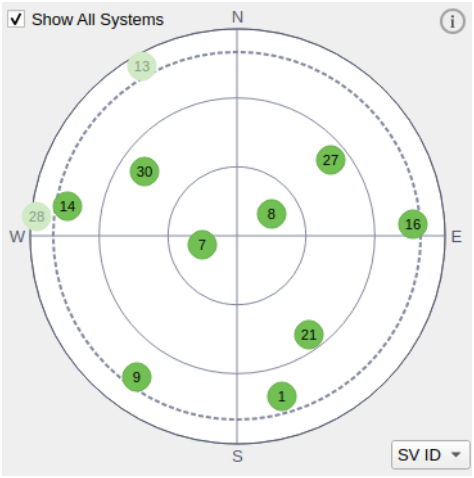

Fig. 2. Sky view with visible GPS satellites.

different received components to filter out undesired signals.

B. Preprocessing & Beamforming Module

Due to Skydel's internal logic, each of the generated contributions, GPS signals and interference, is stored in separate I/Q files. As a result, each instance produces two output files that must be combined to reproduce the actual signal as perceived in the presence of an interference.

However, prior to merging both contributions, we measure the power levels of the individual components to ensure a specific jamming-to-signal ratio (J/S) in the resulting signal.

By comparing the interference power, $P_{\text{J}_{\text{dB}}}$, with the power measured for the GPS signals, $P_{\text{GPS}_{\text{dB}}}$, we define a scaling factor β as,

$$\beta = 10^{\left(J/S - (P_{\text{J}_{\text{dB}}} - P_{\text{GPS}_{\text{dB}}})\right)/20}, \tag{5}$$

ant the output signal from the l-th instance for the case of a single interference ($M = 1$) is obtained as,

$$\left[\mathbf{x}^{(\text{NF})}[n]\right]_l = \sum_{v=1}^{V} \left[\mathbf{a}(\varphi_s, \theta_v)\right]_l s^{(v)}[n] + \beta \left[\mathbf{a}(\varphi_i, \theta_i)\right]_l i[n]. \tag{6}$$

Note in (6) that $\left[\mathbf{x}^{(\text{NF})}[n]\right]_l$ does not include the noise contribution, it is noise-free. Although Skydel offers the option of introducing Gaussian noise into the simulated GPS signals, this setting was disabled for this analysis. The reason behind this is that the noise generated across different Skydel instances is correlated, leading to correlated noise across the antenna elements in our simulation. This does not represent a real antenna array, where noise is spatially white, therefore we generate noise-free GPS signals using Skydel and manually add the noise component.

Using a predefined representative signal-to-noise ratio (SNR), the noise power is computed as,

$$P_{\text{n}} = P_{\text{GPS}} \left(\text{SNR}|_{\text{lin}}\right)^{-1}, \tag{7}$$

where $\text{SNR}|_{\text{lin}}$ is the SNR in linear scale. Therefore, the noise term to be added to the l-th instance output, $\left[\mathbf{x}^{(\text{NF})}[n]\right]_l$, is obtained as shown in (8), where `randn()` is a built-in Matlab function that generates random numbers following a Gaussian distribution.

$$\left[\mathbf{n}[n]\right]_l = \sqrt{\frac{P_{\text{n}}}{2}}\Big(\texttt{randn()} + j\texttt{randn()}\Big). \tag{8}$$

With the noise incorporated into the simulation, the output signal from each instance is treated as the data received by a real antenna channel. These signals are arranged into matrix $\mathbf{X} \in \mathbb{C}^{L \times N}$, which contains the N samples processed for each of the L instances, i.e., $\mathbf{X} = [\mathbf{x}[0]\ \mathbf{x}[1]\ \ldots\ \mathbf{x}[N-1]]$. Referring to the diagram in Fig. 1, in the analysis of the four-element array, matrix $\mathbf{X}$ is composed of the signals in *data_ant_1*, *data_ant_2*, *data_ant_3*, and *data_ant_4*, whereas when only two antennas are considered, the rows of matrix $\mathbf{X}$ are constituted only by *data_ant_1* and *data_ant_2*.

The next step is to build the weights for the two techniques analyzed in this work, PI and CAP. The implementation of the PI beamformer is straightforward once $\mathbf{X}$ is available, since the only information needed to perform the calculation in (3) is $\mathbf{R}_{\mathbf{x}}$, computed as $\mathbf{R}_{\mathbf{x}} = \frac{1}{N}\mathbf{X}\mathbf{X}^H$. However, the implementation of the CAP beamformer is slightly more complex. Since the distortionless constraint must be maintained for each visible satellite, we must generate as many sets of weights as satellites are available in the simulation. To do so, the V steering vectors $\mathbf{a}(\varphi_v, \theta_v), v = 1, \ldots, V$, must be built using the angular information retrieved from the Skydel simulator. As previously introduced, Skydel provides the needed azimuth and elevation values, thus we use it to construct the steering vectors as,

$$\mathbf{a}(\varphi_v, \theta_v) = \exp\left(-j\frac{2\pi}{\lambda}\mathbf{Q}^T \begin{bmatrix} \sin(\varphi_v)\sin(\theta_v) \\ \cos(\varphi_v)\sin(\theta_v) \\ \cos(\theta_v) \end{bmatrix}\right), \tag{9}$$

where $\mathbf{Q} \in \mathbb{R}^{3\times L}$ is a matrix containing the 3D coordinates, (x, y, z), of each antenna in the array with respect to the reference element, $(0, 0, 0)$. In this analysis, we assume a uniform linear array (ULA) where the antennas are placed along the x-axis. Under these circumstances, the l-th column of matrix $\mathbf{Q}$ is defined as $[\mathbf{Q}]_{:,l} = \lambda/2\,[l, 0, 0]^T, l = 0, \ldots, L-1$. Taking this into consideration, the V weight vectors for the CAP beamformer are directly computed according to (4).

C. FGI-GSRx GNSS Software Receiver

After applying the PI weights, the beamformer output is the interference-free signal, represented by the $N \times 1$ vector $\mathbf{y}_{\text{PI}}$, which can be directly fed into the FGI-GSRx GNSS software receiver for further processing. However, unlike the PI, the CAP beamformer does not yield a single output signal but rather V, one per satellite, with the v-th signal denoted by vector $\mathbf{y}_{\text{CAP}}^{(v)}$.

When the FGI-GSRx GNSS receiver is launched, the acquisition process begins by loading the data from the specified file. At this stage, no information about the visible satellites is available, therefore a DoA-dependent technique such as the CAP beamformer cannot be applied. However, if the interference is not mitigated before the receiver starts this process, no GPS signals will be detected. This highlights the need to apply a technique that can attenuate the interference without relying on additional information, thereby ensuring a successful acquisition process. For this, we use the output of the PI for acquisition, which allows us to obtain the necessary information to potentially exploit the CAP technique.

Once acquisition is completed, the parameters estimated are used to initiate the tracking stage. Each acquired satellite is tracked using an independent channel. By default, the FGI-GSRx receiver uses the same file used for acquisition to carry out the tracking across all the channels. However, to asses the performance of the CAP beamformer, which applies DoA-dependent weights for each satellite, we must modify the tracking module to contemplate the use of a different file for each channel. In this modified version of the FGI-GSRx receiver, each tracking channel can be associated with a specific data file, which allows us to link the channel tracking the v-th satellite to the corresponding beamformer's output.

Therefore, regardless of the technique applied during the tracking stage, acquisition is always performed on the signal obtained after applying the PI, ensuring interference mitigation and thus enabling the proper retrieval of GPS signals. Subsequently, when tracking begins, the beamformer can either be switched to the CAP, since the satellites are known, or remain set to the PI.

The resulting testbed enables a valuable analysis of the two techniques without requiring any additional hardware beyond

the Skydel simulator itself. Through the implemented module we adapt Skydel's outputs to emulate a real multi-antenna GNSS receiver, and the modifications introduced in the FGI-GSRx receiver enable the processing of outputs from DoA-dependent beamformers, allowing us to obtain meaningful performance metrics.

IV. Experimental Results

The results presented in this section aim to validate the previously described testbed and to report the performance of the two proposed techniques, PI and CAP, in GNSS handheld receivers. Since the focus of this work is on small devices, the experiments performed are limited to the case of two and four antennas, where we deploy both algorithms and study their behavior in the presence of a continuous wave (CW) interference. The analysis considers GPS L1 C/A signals affected by a CW at the central frequency of the band, i.e., $f_c = 1575.42$ MHZ. The interference power is set to produce a J/S of 50 dB at the receiver, while a SNR value of -19 dB is assumed for noise generation [20].

The disposition of the satellites at the time of the simulation is that shown in Fig. 2. The azimuth angle, φ, is measured in the horizontal plane with respect to an imaginary reference line pointing north from the receiver, which is defined as $\varphi = 0°$. Positive azimuth angles are measured clockwise, while negative angles are measured counterclockwise. Based on this convention, the interference transmitter is positioned 200 m from the receiver at an azimuth angle of $\varphi_i = -66.94°$, as illustrated in Fig. 3.

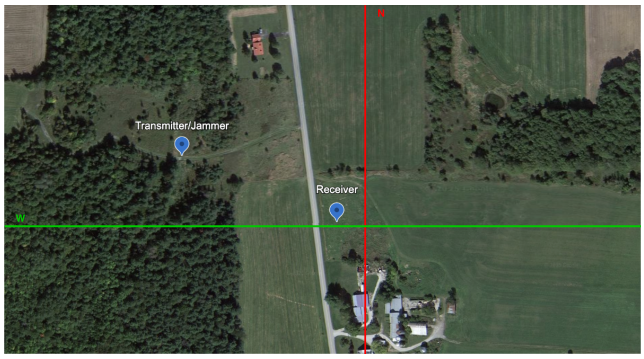

Fig. 3. Position of the interference transmitter with respect to the receiver.

To validate the proposed architecture, we first estimate the DoA of the interference to ensure that accurate spatial information can be extracted from the Skydel setup. We use the four-antenna configuration along with the CAP for DoA estimation, which measures the output power in all the array directions after applying their corresponding weights. The resulting function exhibits as many peaks as signals are observed, with these maximum values directly linked to the received power of each contribution. Since only one CW interference is present alongside the GPS signals, which remain buried below the noise floor, we expect to observe a single prominent peak, corresponding to the estimated DoA.

The results obtained from this analysis are presented in Fig. 4, where a red-dashed line indicating the true DoA of the interference is included for reference. As seen, the estimated DoA, $\hat{\varphi} = -67.66°$, is very close to the true value, with an error of less than $1°$. This suggests that the proposed Skydel-based setup is well-suited for accurate multi-antenna simulations.

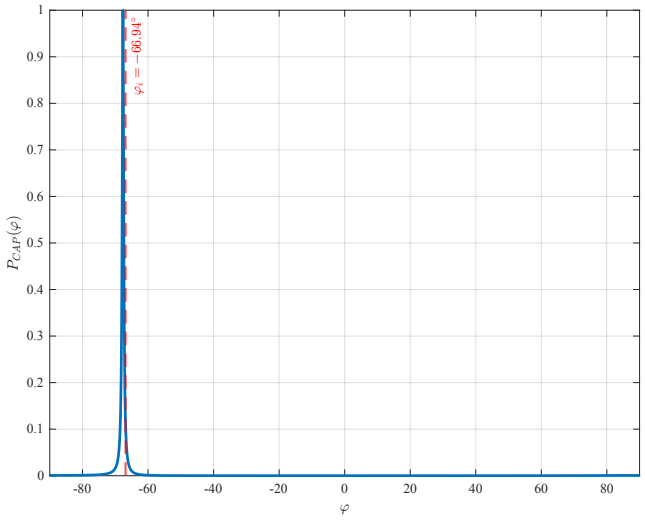

Fig. 4. Output power of the CAP beamformer for different φ.

Nevertheless, our objective is to use the presented testbed to evaluate the impact of the PI and CAP, focusing on metrics that offer real insight into the receiver's behavior. To this end, we rely on the information reported by the FGI-GSRx receiver after processing 65 s of the outputs of both techniques for the two- and four-element antenna array configurations. Particularly, for each case, we evaluate the C/N_0 of the tracked satellites and the final error in the positioning solution, as these metrics reflect the receiver's ability to maintain signal tracking and achieve accurate positioning once the interference is mitigated. The scenario with no mitigation technique applied cannot be analyzed, as the receiver becomes saturated when the interference is addressed.

Table I summarizes the results for each technique and array size in terms of number of satellites tracked and horizontal (2D) root mean square error (RMSE) of the positioning solution. The most notable result is that, although the receiver is unable to track all nine satellites in either case, increasing the number of antennas from two to four allows tracking an additional one, raising the number from seven to eight. This is because a larger array improves interference mitigation, leading to higher C/N_0, which is crucial for satellite acquisition.

This enhancement in terms of C/N_0 is more clearly observed in Fig. 5, where the average C/N_0 among the tracked satellites is presented for each analyzed case. Notably, the CAP beamformer with four antennas demonstrates significantly improved performance, showing an increase of approximately 5 dB-Hz compared to the other cases. This can be explained through the distortionless constraint. Since the CAP technique guarantees

TABLE I
SUMMARY OF TRACKED SATELLITES AND 2D RMSE.

	2 Antennas		4 Antennas	
	Tracked Sat.	**2D RMSE**	**Tracked Sat.**	**2D RMSE**
PI	7/9	4.06m	8/9	3.28m
CAP	7/9	4.38m	8/9	2.28m
Only GPS - Single Antenna				
	Tracked Sat.		**2D RMSE**	
	9/9		3.04m	

a unitary response in the DoA of the satellite, the array pattern does not introduce random gains in that direction, as can happen with the PI. The PI beamformer directly mitigates the undesired contribution without controlling the array pattern's behavior in other DoA, potentially causing aleatory attenuation in desired directions. This also explains why the improvement between the two and four antenna cases in the PI is not as significant as in the CAP. Note that the enhancement observed with the CAP is twofold: it results from both preserving the desired DoA without distortion and increasing the interference mitigation capacity. In contrast, the improvement in the PI is solely attributed to the latter.

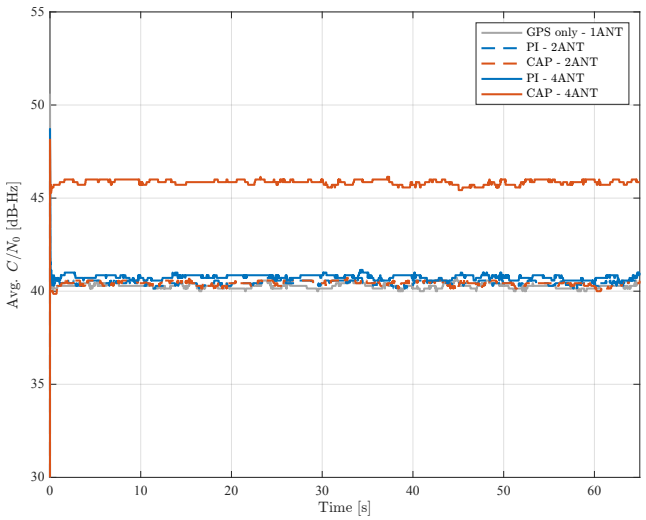

Fig. 5. Average C/N_0 with PI and CAP for 2- and 4-element configurations.

The metrics previously discussed offer valuable insight into the receiver's performance. However, the primary objective of a GNSS receiver is to deliver accurate positioning solutions, making the most relevant performance metric the accuracy of the solution itself. In Fig. 6 the 2D position error for all the cases analyzed is presented, along with the baseline results obtained using only GPS signals (no interference present) in a single-antenna scenario. Furthermore, in the top left corner of the figure, the variance of the results for each case is shown to provide additional clarity on the behavior in each scenario.

The reported results highlight the effectiveness of the beamforming techniques, as the receiver is able to provide positioning solutions with a 2D error consistently below 10 m

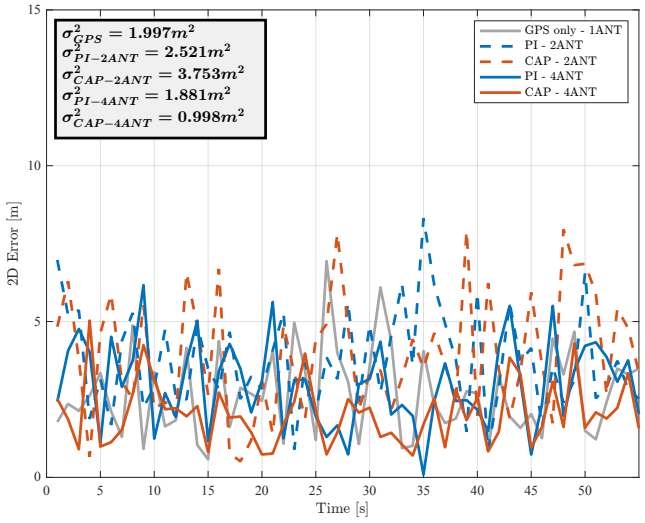

Fig. 6. 2D error in the positioning solution with PI and CAP for 2- and 4-element configurations.

in all scenarios. Moreover, when the number of antennas in the array is increased from two to four, the position error drops below 5 m during most time instants.

Overall, the best performance is achieved with four antennas using the CAP technique, $\sigma^2_{CAP-4ANT} = 0.998m^2$, which is in line with the tracking results presented in Fig 5. However, when only two antennas are used, the performance of the PI ($\sigma^2_{PI-2ANT} = 2.521m^2$) is better than that of the CAP beamformer ($\sigma^2_{CAP-2ANT} = 3.753m^2$), offering slightly smaller positioning errors. This indicates that both beamforming techniques are effective at mitigating interference, even when the number of antennas is limited. In particular, the PI technique offers competitive results with fewer antennas, while the CAP technique further improves performance as the array size increases.

V. CONCLUSION

In this paper, we have demonstrated the feasibility of using the Skydel simulator to assess the performance of beamforming techniques in GNSS multi-antenna receivers. The developed preprocessing and beamforming module adapts Skydel's output to emulate an antenna array, while the modifications introduced in the FGI-GSRx receiver enable the processing of the beamformer's output and the extraction of valuable performance metrics. Using the proposed setup, we have analyzed the CAP and PI techniques in constrained scenarios where the number of antennas was limited to, at most, four. The results obtained not only validate the suitability of the architecture, but also highlight the potential of beamforming methods to enhance GNSS receiver performance. Even with a limited number of antennas, these techniques effectively mitigate interference, making them viable solutions for resource-constrained systems, such as handheld devices.

REFERENCES

[1] D. Egea-Roca, M. Arizabaleta-Diez, T. Pany, F. Antreich, J. A. López-Salcedo, M. Paonni, and G. Seco-Granados, "GNSS user technology: State-of-the-art and future trends," *IEEE Access*, vol. 10, pp. 39 939–39 968, 2022.

[2] C. Vegni and A. Neri, "GNSS interference: Effects and solutions," in *Proc. ION Pacific PNT*, Honolulu, HI, USA, Apr. 2015, pp. 454–469.

[3] P. Craven, R. Wong, N. Fedora, and P. Crampton, "Studying the effects of interference on GNSS signals," in *Proc. ION International Technical Meeting*, San Diego, CA, USA, Jan. 2013, pp. 893–186.

[4] D. L. Wu. (2024) Innovation: Recent GPS jamming in regions of geopolitical conflict. [Online] Available: https://www.gpsworld.com/innovation-recent-gps-jamming-in-regions-of-geopolitical-conflict/.

[5] D. Robinson. (2024) GPS interference now a major flight safety concern for airline industry. [Online] Available: https://www.theregister.com/2024/01/29/satellite_navigation_jamming_now_a/.

[6] D. L. Wu and J. H. S. Cornelius Csar, "GPS jamming: A historical record from global radio occultation (RO) observations," in *Proc. ION GNSS+*, Baltimore, MD, USA, Sep. 2024, pp. 781–795.

[7] K. Sun, B. Yu, L. Xu, M. Elhajj, and W. Yotto Ochieng, "A novel GNSS anti-interference method using fractional fourier transform and notch filtering," *IEEE Trans. Instrum. Meas.*, vol. 73, pp. 1–17, 2024.

[8] K. Sun, M. Elhajj, and W. Y. Ochieng, "A GNSS anti-interference method based on fractional fourier transform," *IEEE Trans. Aerosp. Electron. Syst.*, vol. 60, no. 5, pp. 5636–5650, 2024.

[9] R. Morales-Ferre, P. Richter, E. Falletti, A. de la Fuente, and E. S. Lohan, "A survey on coping with intentional interference in satellite navigation for manned and unmanned aircraft," *IEEE Commun. Surveys Tuts.*, vol. 22, no. 1, pp. 249–291, 2020.

[10] A. L. Swindlehurst, B. D. Jeffs, G. Seco-Granados, and J. Li, "Applications of array signal processing," in *Academic Press Library in Signal Processing: Volume 3*, ser. Academic Press Library in Signal Processing. Elsevier, 2014, vol. 3, ch. 20, pp. 859–953.

[11] R. G. Lorenz and S. P. Boyd, "Robust beamforming in GPS arrays," in *Proc. ION National Technical Meeting*, San Diego, CA, USA, Jan. 2002, pp. 409–427.

[12] M. Sahmoudi and M. G. Amin, "Optimal robust beamforming for interference and multipath mitigation in GNSS arrays," in *Proc. IEEE International Conference on Acoustics, Speech, and Signal Processing - (ICASSP '07)*, vol. 3, Honolulu, HI, USA, Apr. 2007, pp. III–693–III–696.

[13] M. Sgammini, F. Antreich, L. Kurz, M. Meurer, and T. G. Noll, "Blind adaptive beamformer based on orthogonal projections for GNSS," in *Proc. ION GNSS*, Nashville, TN, USA, Sep. 2012, pp. 926–935.

[14] M. Mañosas-Caballú, J. López Vicario, and G. Seco-Granados, "On the performance of deterministic beamformers: A trade-off between array gain and attenuation," *Signal Processing*, vol. 94, pp. 158–162, 2014.

[15] G. Foreman-Campins, L. Pallaré-Rodríguez, S. Locubiche-Serra, G. Seco-Granados, and J. A. López-Salcedo, "Methodologic assessment of beamforming techniques for interference mitigation on GNSS handheld devices," in *Proc. 2023 International Conference on Localization and GNSS (ICL-GNSS)*, Castellón, Spain, Jun. 2023, pp. 1–7.

[16] L. Pallarés-Rodríguez, D. Gómez-Casco, N. Bni-Lam, G. Seco-Granados, J. A. López-Salcedo, and P. Crosta, "Low cost SDR for GNSS interference mitigation using spatial diversity techniques," *Engineering Proceedings*, vol. 88, 2025.

[17] FGI-GSRx software receiver. [Online] Available: https://github.com/nlsfi/FGI-GSRx.

[18] R. Compton, "The power-inversion adaptive array: Concept and performance," *IEEE Trans. Aerosp. Electron. Syst.*, vol. AES-15, no. 6, pp. 803–814, 1979.

[19] R. Lorenz and S. Boyd, "Robust minimum variance beamforming," *IEEE Trans. Signal Process.*, vol. 53, no. 5, pp. 1684–1696, 2005.

[20] K. Borre, I. Fernández-Hernández, J.A. López-Salcedo, and M.Z.H. Bhuiyan, *GNSS Software Receivers*. Cambridge University Press, 2022.